Heliyon 10 (2024) e38050

Contents lists available at ScienceDirect

Heliyon

journal homepage: www.cell.com/heliyon

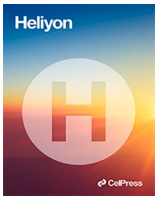

Research article

Ulinastatin modulates NLRP3 inflammasome pathway in PTZ-induced epileptic mice: A potential mechanistic insight

Huan Wang [a], Yuzhu Ma [b], Dongmei Jin [a], Xinlei Yang [c], Xiangping Xu [b,*]

[a] Department of Neonatology, The First Affiliated Hospital of Harbin Medical University, Harbin, Heilongjiang, China
[b] Department of Pediatrics, The First Affiliated Hospital of Harbin Medical University, Harbin, Heilongjiang, China
[c] The First Affiliated Hospital of Harbin Medical University, Harbin, Heilongjiang, China

ARTICLE INFO

Keywords:
Epilepsy
NLRP3 inflammasome
Neuroinflammation
Blood-brain barrier
Ulinastatin

ABSTRACT

Objective: The NLRP3 (NOD-like receptor family, pyrin domain containing 3) inflammasome-driven immune-inflammatory response has been shown to play a critical role in epilepsy progression across multiple studies. While Ulinastatin (UTI), an immunomodulatory agent known to target the NLRP3 pathway in neurological disorders, its implications in epilepsy have not been extensively studied. This investigation aims to explore UTI's role and underlying mechanisms in epilepsy.

Methods: To assess UTI's effects on epilepsy severity, neuroinflammation, and BBB integrity, a pentylenetetrazole (PTZ)-induced epilepsy model in mice and a co-culture system involving BV2 and HT22 cells stimulated by lipopolysaccharide (LPS) and ATP were employed. Techniques utilized included qPCR, Western blotting, ELISA, immunohistochemistry (IHC) staining, Evans Blue dye extravasation, glutamate assays, the Morris water maze, and Annexin V apoptosis assays.

Results: In the PTZ model, UTI administration led to a substantial decrease in seizure intensity and susceptibility, inhibited NLRP3 inflammasome activation, reduced neuroinflammatory interactions, lowered hippocampal and systemic inflammatory mediator levels, and improved cognitive performance. Furthermore, UTI upregulated claudin-5 expression, a tight junction protein in the endothelium, and diminished Evans Blue dye leakage, indicating improved BBB integrity. In BV2 and HT22 cell co-culture models, UTI exerted neuroprotective effects by mitigating microglia-mediated neurotoxicity and fostering neuronal recovery.

Conclusions: The findings demonstrate that UTI exerts transformative regulatory effects on the NLRP3 inflammasome in epilepsy models. This intervention effectively suppresses neuroinflammation, lessens seizure severity and susceptibility, and ameliorates epilepsy-related BBB dysfunction and cognitive impairments.

1. Introduction

Epilepsy, a prevalent neurological condition affecting individuals of all ages, is estimated to have a global incidence rate of roughly 1 %. Its aftermath is often associated with cognitive deficits and various psychiatric conditions [1]. Characterized by unprovoked, recurrent, and persistent seizures, epilepsy affects a significant proportion of the population, with approximately one-third of patients necessitating pharmacological interventions. The disorder intertwines elements of neurobiology, cognitive research, and

* Corresponding author.
E-mail address: xxp562005@163.com (X. Xu).

https://doi.org/10.1016/j.heliyon.2024.e38050
Received 6 June 2024; Received in revised form 3 September 2024; Accepted 17 September 2024
Available online 19 September 2024

psychosociological aspects [1]. Despite extensive efforts, the underlying mechanisms of epilepsy continue to be a subject of active investigation.

Hence, Elucidating the mechanisms underlying drug-resistant epilepsy and improving patients' well-being and survival rates are crucial for the development of innovative therapeutic approaches. Recent research has implicated neuroinflammation in the initiation and progression of epilepsy [1,2]. This phenomenon arises from the intricate interplay within both central and peripheral immune niches, encompassing neurons, microglia, astrocytes, and the blood-brain barrier (BBB) [3,4]. The dynamic interplay between microglia and astrocytes is central to neuroinflammation, a key component of the immunological landscape in epilepsy, as evidenced in temporal lobe epilepsy cases through the modulation of signaling pathways such as NF-κB and NLRP3 [5,6].

These changes can lead to abnormal neuronal excitability, intensified inflammatory reactions, modifications indrug transport proteins, heightened glutamate secretion, and blood-brain barrier disruption, collectively contributing to drugresistance and the exacerbation of epilepsy [6,7].

Regarding the NLRP3 inflammasome's initiation and activation, components of this complex involve TWIK2 (two-pore domain weakly inwardly rectifying potassium channel 2), P2X7 (P2X purinoceptor 7), ROS (reactive oxygen species), GSDMD-N (gasdermin D N-terminal domain), TLR4 (Toll-like receptor 4), TNF-α (tumor necrosis factor-alpha), TNFR (tumor necrosis factor receptor), and IL-1R (interleukin-1 receptor). The NLRP3 inflammasome plays a crucial role in innate and adaptive immunity, governing inflammation in health and disease scenarios [8]. Its activation encompasses two main stages: initiation and activation (Fig. 1). During these stages, cytokine receptors and TLRs (such as TNF receptors and IL-1R) recognize PAMPs (like TNF-α and LPS) or DAMPs, which can also induce apoptosis, leading to TLR4 stimulation. This results in increased NLRP3 transcription and NF-κB nuclear translocation [9]. NLRP3 then moves to subcellular compartments, forms inflammasomes, activates caspase-1 and releases IL-1β and IL-18 [13]. This cascade amplifies NLRP3 inflammasome activation, promotes cell pyroptosis, and accelerates the release of inflammatory mediators [10].

Individuals with temporal lobe epilepsy prominently stimulate NLRP3 inflammasomes in their brain tissue [11,12]. Research has shown that valproic acid can reduce NLRP3 and ASC levels, effectively controlling seizures [13]. A wealth of evidence from different animal models underscores the critical role of inflammasomes in epilepsy [14]. Dietary DHA and EPA have demonstrated efficacy in Pentylenetetrazol-encouraged epileptic mice via inhibiting activation of NLRP3 and preventing epileptic manifestations [15]. In a rat model of amygdala ignition, targeting NLRP3 and caspase-1 genes with siRNA can reduce seizure activity [16]. IL-1R antagonists and monoclonal antibodies targeting the NLRP3 pathway effectively manage refractory status epilepticus [17]. Current anti-inflammatory treatments for epilepsy in clinical practice, such as NSAIDs and corticosteroids, can alleviate or prevent seizures in children with epilepsy [18–20], yet their therapeutic efficacy in epilepsy patients remains limited.

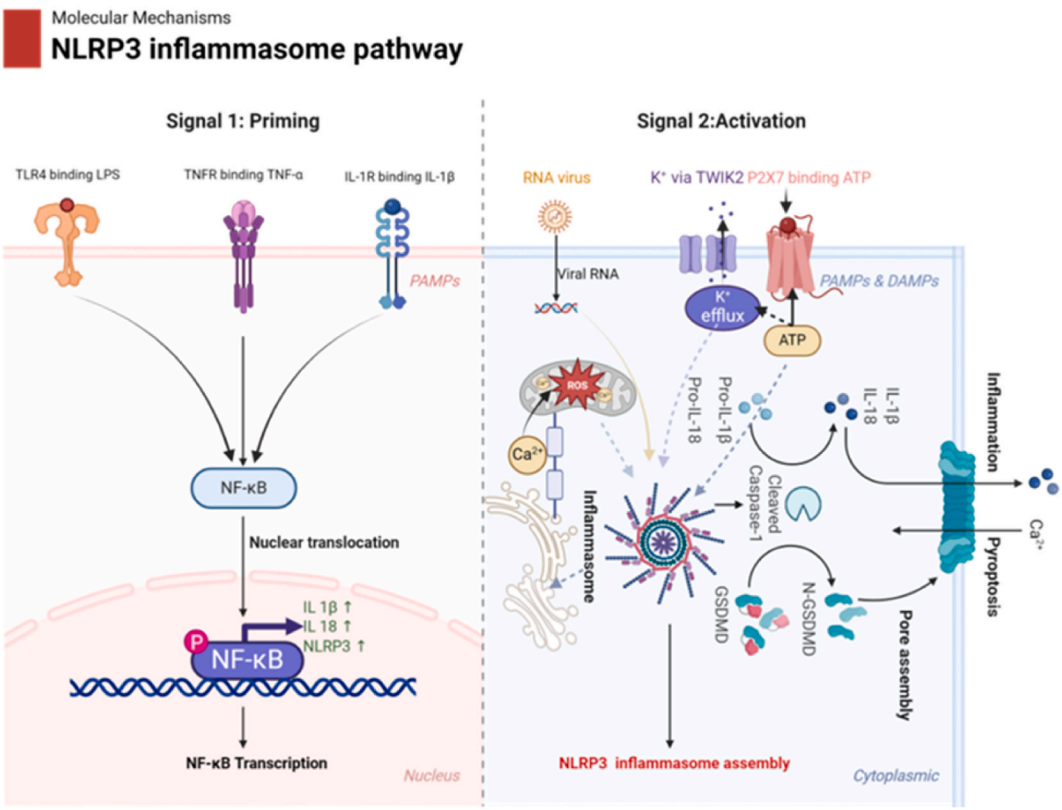

Fig. 1. NLRP3 inflammasome molecular mechanism -signaling pathway.

Serine protease inhibitor ulinastatin (UTI) is well-known for its anti-inflammatory & anti-proteolytic qualities. It also functions as an immunological modulator of the immune response in both the central & peripheral nervous systems [21]. UTI has shown neuroprotective ability in various neurological diseases, such as cerebral ischemia, autoimmune encephalomyelitis, spinal cord injury, hepatic encephalopathy, and hypoxia [22–26]. Studies suggest that UTI can directly inhibit the NLRP3 signaling pathway, revealing its potential for modulating epileptic seizures [27–29].

Few studies have documented the preventive effect of UTI on epilepsy, & its root cause is still unknown. To develop novel treatment approaches for epilepsy and associated disorders, this study investigated the protective impact of UTI on epilepsy linked to the NLRP3 inflammasome. This study used a well-established co-culture system of BV2-HT22 cells produced by LPS-ATP and a PTZ kindling paradigm in mice, after which the animals received UTI.

2. Materials & methods

2.1. Design of experiments & animals

All experiments were performed in the Laboratory Animal Center of the First Affiliated Hospital of Harbin Medical University from January 6, 2022 to July 6, 2023. Eight weeks old and weighing between 20 and 25 g, we acquired healthy adult male C57BL/6J mice [NO. SCXK2020-0001] from Liaoning Changsheng Biotechnology Co., Ltd. Individual housing with a 12-hrs light/dark cycle, pathogen-free conditions, & a consistent temperature range of 20–25 °C was provided for each mouse. This work adhered to the NIH standards for the use and welfare of laboratory animals and was authorised by the Ethics Committee of the First Hospital of Harbin Medical University (IACUC: 2021127). Animals were euthanized for tissue sampling and analysis. Following animal care and protection rules, a deep state of anaesthesia was achieved during euthanasia by administering an intraperitoneal injection of sodium pentobarbital at a dosage of 100 mg/kg. This approach effectively minimised any pain experienced by the animals.

A total of 256 C57BL/6J mice were randomly divided into four equal groups, each consisting of 64 animals: a control group, a PTZ group, a UTI + PTZ group, and a UTI group. The PTZ group was specifically designated for the induction of an epilepsy model through the administration of pentylenetetrazole (PTZ) (sigma, P6500) with an intraperitoneal injection at a dose of 35 mg/kg every other day [30] (Fig. 2). This protocol was based on earlier research. Every day, an intraperitoneal injection of UTI (H032305263, Guangdong Tianpu Biochemical Pharmaceutical Company) solution (50,000 units/kg) was administered to the UTI cohort. The UTI + PTZ group received a daily intraperitoneal injection of UT I (50,000 units/kg) [31](Fig. 2); on the days of PTZ injection, a 1 h following the UTI injection, intraperitoneal PTZ (35 mg/kg) was given. The control group was given equal amounts of saline and PBS. After injecting PTZ, the mice were monitored for 30 min using the modified Racine scoring system (Table 1).

The occurrence of three consecutive seizures graded at grade IV or above verified the animal model's successful establishment. The Racine scores (n = 16) were recorded during 15 PTZ administrations in detail, as well as the latency to stage III (n = 16) and stage V (n = 8) seizures for the first time.

After the model was successfully established, the animals were subjected to further experimental treatments. The mice in the Morris water maze test were put to death 24 h after the 7-day trial was over. The animals were euthanized using an overdose of anesthetics, followed by rigorous cardiorespiratory monitoring to confirm death, in strict adherence to the guidelines set by the Institutional Animal Care and Use Committee (IACUC) for humane endpoints and ethical practices. Subsequently, specific organs relevant to the study objectives were surgically excised under sterile conditions. These included the brain, liver, kidneys, spleen, and, given the focus on epilepsy research, the hippocampus. Harvested organs were promptly preserved to maintain tissue integrity: brains, livers, and kidneys were fixed in 10 % buffered formalin for histological assessment, while the spleen and hippocampus were flash-frozen in liquid nitrogen for subsequent biochemical and molecular analyses.

2.2. Cell Lines, Culture, and Chemicals

The mouse-derived BV2 microglial cells & HT22 neuronal cell lines were generated from the Pricella Life Science & Technology Co., Ltd., Wuhan, China. The separate cultures of the BV2 & HT22 cell lines were maintained in DMEM high-glucose medium, with additions of 10 % fetal bovine serum (DL-FSP500, ExCell Bio)& 1 % penicillin-streptomycin(15140-122, Gbico). Cultures were painstakingly maintained at a constant 37 °C in an atmosphere with 5 % CO_2. Experimental cells were selected from within their 10th passage to ensure consistent cellular properties.

ATP (B2176, MCE, China) was purchased from Med Chem Express LPS (L 3012, Sigma-Aldrich, USA) was obtained fromSigma-

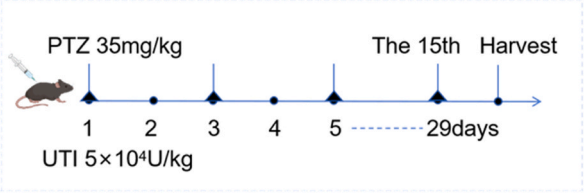

Fig. 2. Animal experimental protocol.

Table 1
Modified racine score.

Stage	Feature	Score
I	Reduced activity, often stationary in the corner of the observation chamber.	1
II	Minor whole-body twitches, variable movement.	2
III	Clonus in one or both forelimbs, with or without Straub's tail.	3
IV	Bilateral hind limbs clonic seizures, extend the hind limbs backwards and parallel to the surface	4
V	Generalized tonic-clonic seizures, possibly including intense jumping, running, and loss of posture.	5
VI	Hind limb extension leading to death.	6

Aldrich.

2.3. BV2-HT22 co-culture system

Using the conditioned medium (CM) transfer approach, a BV2-HT22 co-culture system was set up. BV2 cells were subjected to a 24 h treatment of 1 μg/ml LPS, succeeded by a 2 h treatment with gradient doses of ATP (0.1, 1, 3, 5 mM). The cells were incubated for a further 24 h after being switched to a new media. The supernatant was collected as CM under various ATP concentration settings after the extracellular fluid was spun for 10 min at 1000 rpm.

After being planted onto sterile 96-well plates, HT22 cells (5×10^3 cells per well) were subjected for a full night. To assess the neurotoxicity in the LPS-ATP group, the medium in HT22 cells was replaced with CM prepared by treating BV2 cells with 1 μg/ml LPS & gradient deliberations of ATP (0.1, 1, 3, 5 mM), using 0.1 % DMSO in DMEM as a control, and incubated for 24 h. In the UTI-LPS-ATP group, the effect of UTI on HT22 neurotoxicity was assessed by pre-treating with 1000 U/ml UTI for 1 h under the same conditions. Next, the CCK8 test (Seven, China) was used to quantify cell viability. 10 μL of CCK8 solution was added to each well, and the optical density at 450 nm (OD450) was determined during a 3 h incubation period.

The ATP concentration (5 mM) that reduced HT22 cell viability by approximately 50 % was selected as the optimal intervention concentration.

Three sets of cells were created: LPS-ATP, UTI-LPS-ATP, & vehicle. In the Vehicle group, HT22 neurons were cultured without any intervention (e.g., CM or UTI). In the LPS-ATP group (Fig. 3), the medium of HT22 neurons was replaced with CM prepared with LPS(1 μg/ml) and the determined concentration of ATP(5 mM), & A whole day was spent incubating the cells. In the group UTI-LPS-ATP, 1000 U/ml UTI was added 1 h before the addition of CM (Fig. 3).

2.4. Flow cytometry annexin V-FITC/PI staining

HT22 cells were cultured in a conditioned co-culture for 24 h before evaluating apoptosis employing the Annexin V-FITC/PI apoptosis diagnostic kit (AP101C, Liankebio). Following treatment with 0.25 % trypsin in the absence of EDTA, cells were collected by centrifugation at 4 °C for 5 min at 3000 rpm. Then around 10^5 cells were resuspended in 500 μL of Binding Buffer. The cells were then

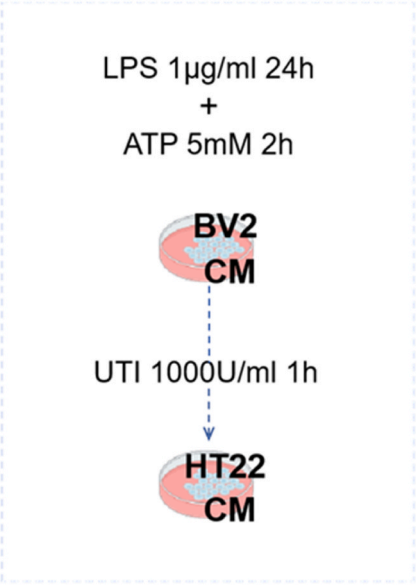

Fig. 3. Co-Culture Model protocol.

filtered to produce a single-cell solution, and they were stained with 5 μL of Annexin V-FITC and 10 μL of PI. Subsequently, the cells were placed in a dark environment at room temperature and left undisturbed for 5 min.

The overall apoptosis rates (early plus late apoptosis) were determined by using flow cytometry to identify the fluorescence of FITC (excitation = 488 nm, emission = 530 nm) and PI (excitation = 535 nm, emission = 615 nm). FlowJo software was utilized for data analysis and graphical presentation.

2.5. Real-time quantitative PCR (qPCR)

Hippocampal tissue & cell samples were subjected to RNA extraction utilizing Trizol reagent (SM132, Seven Bio, China). The RNA concentration was measured and normalized. The RNA of NLRP3, ASC, caspase-1, NF-κB, TNF-α, IL-18, & IL-1β was reverse transcribed into cDNA using a reverse transcription kit (A2791, Promega, USA) using the primers provided in Table 2 that were synthesised by Sangon Biotech (Shanghai, China). Amplification was performed using a qPCR kit (SM143, Seven Bio, China) with GAPDH as the internal control for annealing and extension. Amplification specificity was confirmed by melting curve analysis. After being gathered, the experimental data were computed using the 2-ΔΔCt technique and subjected to statistical analysis.

2.6. Protein isolation and Western blotting

The RIPA buffer, which included phosphatase inhibitors and PMSF (Beyotime, Jiangsu, China)was employed for obtaining whole proteins from both the HT22 cells and hippocampal tissues. The same mixture was used for the total protein extraction steps from HT22 cells. The protein concentrations were measured using the BCA kit (Beyotime, Jiangsu, China). The wet transfer machine (40D, Beijing Liuyi) (300 mA, 120 min) transfers equal quantities of protein (30 μg per lane) onto PVDF membranes (Merck Millipore). The protein was separated by SDS-PAGE (5 % stacking gel, 80 V, 30 min; 10–12.5 % separating gel, 130 V, 50 min). The membranes were blocked using the following primary antibodies for 1.5 h at room temperature with 5 % skim milk. They were then incubated overnight at 4 °C: Rabbit anti-ASC (1:1000, bs-6741R, Bioss), rabbit anti-NLRP3 (1:1000, 19771-1-AP, Proteintech), rabbit anti-Caspase-1 (1:1000, 22915-1-AP, Proteintech), rabbit anti-cleaved Caspase-1 (1:50, sc-398715, Santa Cruz), rabbit anti-NF-κB p-p65 (1:1000, 3033T, rabbit anti-NF-κB p65 (1:1000, Cell Signaling Technology), AF1234, Beyotime), mouse anti-GAPDH (1:5000, 60004-1-Ig, Proteintech) and rabbit anti-Claudin-5 (1:1000, ABT45, Abcam).

The membranes were first cleaned three times with TBST (2 % Tween-20), and then they were incubated for 1 h at 4 °C using either goat anti-mouse (1:2000, A0216, Beyotime, China) or goat anti-rabbit (1:2000, A0208, Beyotime, China) secondary antibodies conjugated with horseradish peroxidase (HRP). Immunoreactive bands are visualized using enhanced ECL, scanned with Imaging analysis software (Clinx Scientific Instruments, China), and analyzed with ImageJ, and the relative protein expression levels for each band were statistically analyzed.

2.7. ELISA for inflammatory cytokines

Following sodium pentobarbital anaesthesia, blood was drawn from the animals by heart puncture. The serum was isolated by centrifuging the blood at 1000 rpm for 20 min, which was then kept at −80 °C until it was needed. Using ELISA kits (Elabscience, China), the amounts of TNF-α (MSEL-M0002), IL-18 (EL-M0730), & IL-1β (MSEL-M0003) in mouse serum were determined. The ELISA plate was filled with standards & serum samples in the prescribed order, & it was then maintained for 90 min at 37 °C. The primary antibody was added and allowed to incubate for 60 min after the liquid on the plate was discarded. After washing the plate, 30 min of incubation were spent with the secondary antibody added. To stop the reaction, the substrate was added and thoroughly cleaned before being incubated for 15 min. An optical density (OD) was assessed at 450 nm by using a microplate reader. Statistical analysis

Table 2
Primer Sequences for qPCR Amplification.

qPCR	5′ to 3′
NF-κB F	5′-GACACGACAGAATCCTCAGCATCC-3′
NF-κB R	5′-CCACCAGCAGCAGACATG-3′
NLRP3 F	5′-TGGATGGGTTTGCTGGGAT-3′
NLRP3 R	5′-CTGCGTGTAGCGACTGTTGAG-3′
Caspase-1 F	5′-ATACAACCACTCGTACACGTCTTGC-3′
Caspase-1 R	5′-TCCTCCAGCAGCAACTTCATTTCTC-3′
ASC F	5′-CACAGAAGTGGACGGAGTGC-3′
ASC R	5′-GGTGGTCTCTGCACGAACTG-3′
IL-18 F	5′-ACTTTGGCCGACTTCACTGT-3′
IL-18 R	5′-GGGTTCACTGGCACTTTGAT-3′
TNF-α F	5′-GCCACCACGCTCTTCTGTCT-3′
TNF-α R	5′-TGAGGGTCTGGGCCATAGAAC-3′
IL-1β F	5′-ACCTTCCAGGATGAGGACATGA-3
IL-1β R	5′-AACGTCACACACCAGCAGGTTA-3′
GAPDH F	5′-GCTGGCATTGCTCTCAATGAC-3′
GAPDH R	5′-TCCACCACCCTGTTGCTGTAG-3′

was done after a standard curve was used to determine the sample concentrations.

2.8. Immunohistochemistry (IHC) staining

The brain tissues were covered in paraffin then sectioned to a thickness of 3 μm, and fixed in 4 % paraformaldehyde for 24 h after death before being subjected to IHC staining. After dehydrating coronal slices (3 μm), antigen retrieval was performed with citrate buffer (pH 6.0, P0083, Beyotime) for GFAP and Tris-EDTA (pH 9.0, PR30002, Boster) for Iba-1/NeuN. After being microwave-boiled for 10 min, the sections were blocked at ambient temperature before being incubated in 3 % H_2O_2 to inhibit endogenous peroxidase activity. The following primary antibodies, all from Abcam (UK), were diluted & incubated with the sections for a whole night at 4 °C in PBS (pH 7.4): Iba-1 (ab178846, 1:2000), NeuN (ab177487 1:3000), & GFAP (ab68428, 1:250). Following a thorough PBS wash, the sections were treated for 1 h at 37 °C with an enzyme-labeled high-sensitivity anti-mouse/rabbit IgG polymer (1:100, Kit-5010, Maxim), followed by developed with DAB, dehydrated, and mounted. Images were acquired, and quantitative analysis of the positive cell area percentage (Area%) was performed using ImageJ software (NIH, USA).

2.9. Evans Blue staining

To examine blood-brain barrier (BBB) integrity, 2 h before to death, mice received an intravenous injection of 4 ml/kg of 2 % Evans Blue dye in the tail vein, with visible blue coloration confirming successful injection. Following euthanasia, animals underwent perfusion with ice-cold saline, and unilateral hemisphere issues were harvested. These tissues (50 mg) were homogenized in a ten-fold volume of 50 % trichloroacetic acid. Following 20 min of 4 °C centrifugation at 10,000 rpm, the supernatant was carefully transferred to a fresh tube & anhydrous ethanol was used to dilute it four times. A spectrophotometric measurement was made at 620/680 nm to determine the concentration of Evans Blue. In terms of brain tissue, the data are represented in ng/mg, accurately quantifying the content of Evans blue in brain tissue for statistical analysis.

2.10. Glutamate concentration measurement

A 20 mg hippocampal tissue sample was taken, diluted tenfold, and homogenized. Next, for 10 min at 4 °C, the homogenate was subjected to centrifugation at 10,000 rpm. 50 μL of the supernatant and 150 μL of trichloroacetic acid were combined, and then the combination was subjected to centrifugation at 3000 rpm for 10 min. Each of the standards & samples (50 μL) was put in a UV plate, and 150 μL of reaction working solution was added according to the steps of the glutamate assay kit (E-BC-K118-S, Elabscience). The initial OD values at 340 nm (A1) were measured. After adding 10 μL of enzyme reagent and incubating at 37 °C for 40 min, the OD values at 340 nm (A2) were measured again. Glutamate concentration was calculated using the following formula:

$$\frac{\text{glutamate content}}{(\mu\text{mol/gprot})} = \frac{(\text{Measure A2} - \text{Measure A1}) - (\text{Blank A2} - \text{Blank A1})}{(\text{Standard A2} - \text{Standard A1}) - (\text{Blank A2} - \text{Blank A1})} \times c \times 4^{*} \times f \div C\,\text{pr}$$

where c represents the standard concentration, f is the volume factor, and Cpr is the protein concentration. The glutamate content was converted to μmol/gprot using a standard curve, and the data were statistically analyzed.

2.11. Morris water maze (MWM)

With water in a circular tank of 120 cm in diameter & 60 cm in height, this labyrinth is split into four quadrants (SE, SW, NW, & NE) each with its own set of visual clues. Platform Setup: A 1 cm submerged transparent platform is placed in the tank for animals to locate, associating it with visual cues. Day 1 (Visible Platform Trial): Animals swim freely to find a visibly elevated platform, across four 60-s trials. Days 2–6 (Hidden Platform Trial): The now submerged platform in the target quadrant requires animals, released from randomized quadrants, to locate it in three daily trials, each capped at 60 s. Animals are led to the platform if not found within the time limit. This phase, tracking escape latency, spans five days for evaluating learning ability and directional orientation. Day 7 (Spatial Probe Trial): With the platform removed, animals are released opposite the target quadrant for a 60-s free swim. Time in the target quadrant and crossings are noted to evaluate memory. Trials are interspersed by 45–60 min.

2.12. Statistical analysis

A one-way or two-way ANOVA, Tukey's multiple comparisons test (for multi-group comparisons), mixed-effects models, repeated measurements, dose-response curves, and Student's t-test were the bases for the statistical assessment, which was carried out using GraphPad 9.5.1. Mean ± standard deviation (SD) is the data presentation format. $P < 0.05$ were deemed to indicate significant differences.

2.13. Supplementary material

We provided the full, non-adjusted images for all the cropped, sliced, or combined gel and blot images. These images are now included as supplementary files.

3. Results

3.1. Ulinastatin attenuates epileptic severity and susceptibility in the PTZ model

The findings of the investigation were reported based on the adjusted Racine scores and the duration it took for the initial seizure to advance to stage III or V. The UTI treatment significantly reduced the modified Racine scores during the early stages of PTZ administration (2nd and 6th to 13th injections) (Fig. 4a). Furthermore, as the disease progressed to more severe stages (with Racine scores generally rising to level 4 or above), At the latter phases of administration (the 14th & 15th injections), no discernible changes were found among the group receiving treatment & control groupings ($n = 16$, Fig. 4a). Compared to the PTZ group, UTI treatment significantly prolonged the latency to reach stage III ($n = 16$, $P < 0.001$, Fig. 4b) and stage V ($n = 8$, $P = 0.00087$, Fig. 4c) seizures. Overall, the results suggest that UTI treatment may have a beneficial impact on the early stages of epilepsy development, potentially reducing the vulnerability of the mice to seizures, but this effect may wane as the condition progresses.

3.2. Ulinastatin Inhibits NLRP3 inflammasome activation in the PTZ model

According to our qPCR data, the PTZ group's hippocampal mRNA expression levels of NF-κB, ASC, NLRP3, & Caspase-1 were noticeably higher (Fig. 5a–d). On the other hand, these genes' expression was decreased during UTI therapy. NF-κB activation in epileptic animals was shown by an increase in the ratio of phosphorylated NF-κB p65 (NF-κB p-p65) to non-phosphorylated levels at the protein level, as determined by Western blot (Fig. 5e). The PTZ group showed enhanced expression of the NLRP3 inflammasome & activated Caspase-1, as evidenced by Fig. 5f & g showing elevated protein expression of NLRP3 & ASC & Fig. 5h demonstrates a significant rise in the proportion of cleaved Caspase-1 to pro-Caspase-1. These findings suggest a strong relationship between the start & development of seizures in the PTZ group with the activation of the NLRP3 pathways. In contrast, these outcomes were the opposite in the UTI + PTZ category. Since there were no appreciable differences in the expression of these variables among the control & UTI categories, the UTI had no discernible impact on this pathway under normal circumstances. UTI could prevent this pathway from activating in pathological circumstances. our findings strongly imply that the NLRP3 inflammasome and NF-κB pathways play a pivotal role in the initiation and progression of seizures in PTZ-induced epilepsy, as evidenced by heightened mRNA and protein expression levels. Conversely, UTI therapy effectively counteracts this inflammatory response, as demonstrated by reduced expression

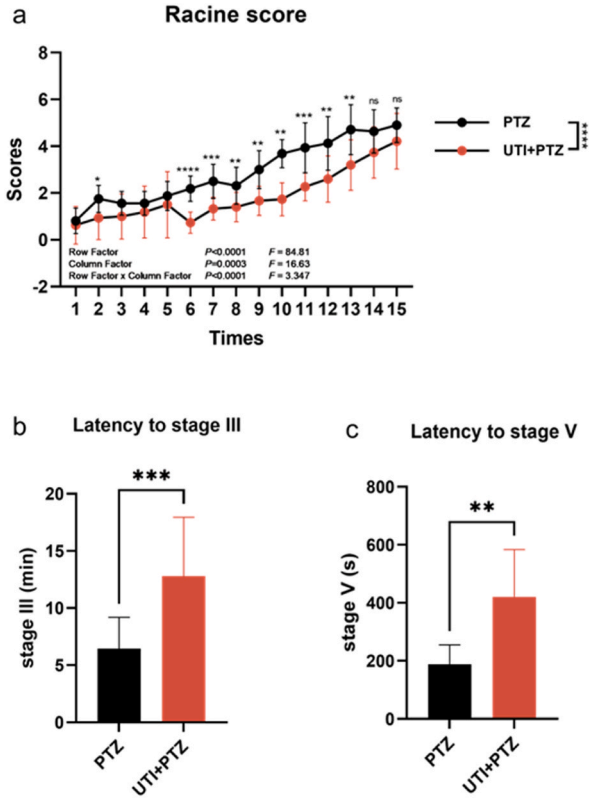

Fig. 4. Impact of UTI on epilepsy susceptibility and severity.
(a) Modified Racine scores among the PTZ & UTI + PTZ categories ($n = 16$) were statistically analyzed. ns, $P > 0.05$; **$P < 0.01$; ***$P < 0.001$; ****$P < 0.0001$. (b) ***$P < 0.001$ for the latency to the first stage III seizure ($n = 16$). (c) *$P < 0.05$ for latency to the first stage V seizure ($n = 8$).

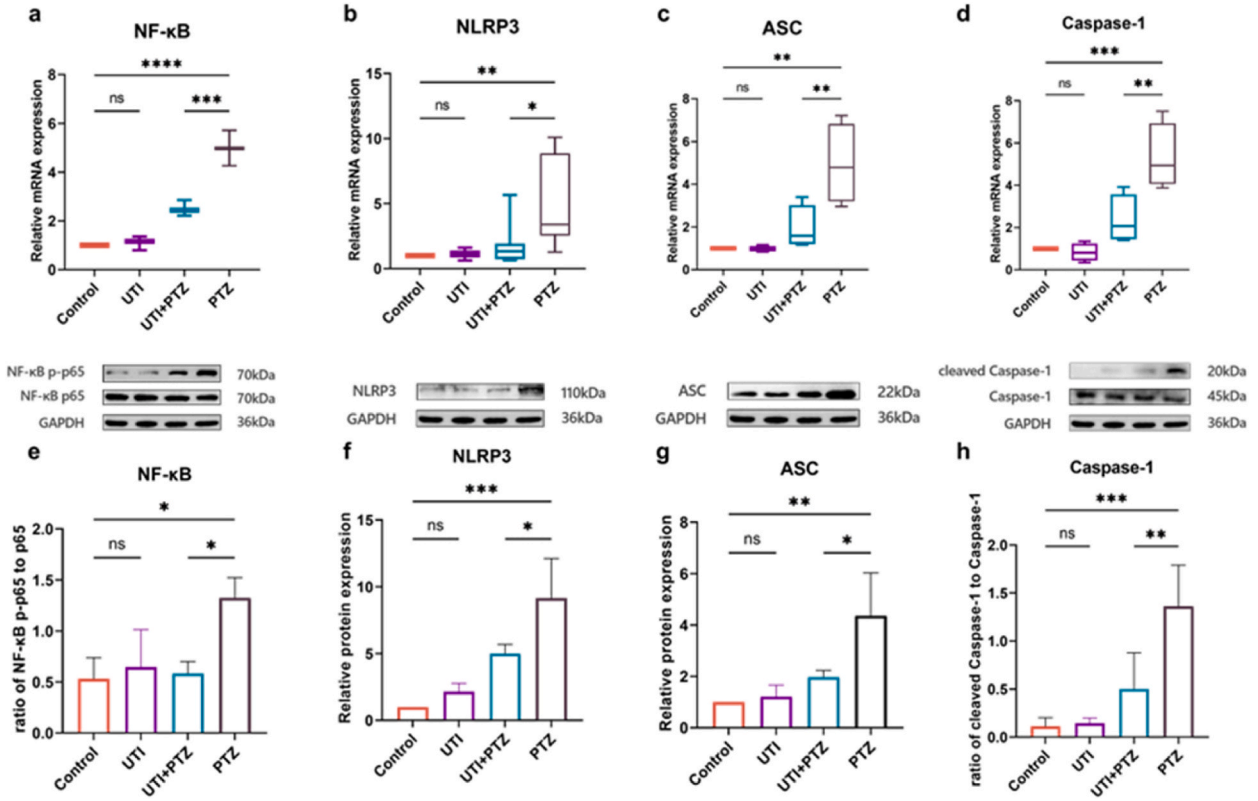

Fig. 5. Ulinastatin inhibits NLRP3 inflammasome activation in the PTZ model.
The NLRP3 inflammasome & NF-κB gene expression were examined using real-time quantitative PCR: Relative gene expression of ASC, Caspase-1, NLRP3, & NF-κB (a-d). The NLRP3 inflammasome & NF-κB protein levels were examined using immunoblotting: (e) The ratio of p65 to phosphorylated NF-κB p-p65. (f–g) NLRP3, ASC, & GAPDH relative quantification ratios. (h) Caspase-1 cleaved form to Caspase-1 ratio. The information is displayed as mean ± standard deviation ($n \geq 3$). *$P < 0.05$, **$P < 0.01$, ***$P < 0.001$, ****$P < 0.0001$; ns, $P > 0.05$. The uncropped and full-size images for (Fig. 5e–h) this figure are provided in Supplementary Fig. S1.

and activation of these pathways, thus suggesting its potential as a therapeutic strategy to alleviate seizure severity.

3.3. *Ulinastatin Modulates Inflammatory Factor Levels and Cognitive Function in the PTZ model*

The levels of central & peripheral inflammatory cytokines were used to evaluate the inflammation in the epilepsy model. The findings demonstrated that in the PTZ category, TNF-α, IL-1β, & IL-18 protein levels in peripheral blood & mRNA levels in the hippocampal regions, as detected by ELISA (Fig. 6a–c), determined by qPCR (Fig. 6d-f), Fig. 6were significantly upregulated (all for $P < 0.05$). On the other hand, UTI decreased these inflammatory cytokine levels, suggesting that UTI lowered neuroinflammation by blocking the NLRP3 inflammasome pathway, which in turn decreased the production of inflammatory cytokines in both the central and peripheral nervous systems.

Neuroinflammation is closely associated with neurodegenerative changes; therefore, cognitive function was assessed using the Morris water maze. The escape latencies of both mice groups decreased as the number of experimental days rose. However, the PTZ group had a higher escape latency compared to the control group ($P < 0.05$) (Fig. 6g), suggesting that their learning ability was impaired. Following UTI therapy, compared to the PTZ category, the escape latency was considerably lower on the fourth day ($P = 0.0241$) & the fifth day ($P = 0.0019$). The PTZ cohort demonstrated a loss in memory ability in the spatial probe test, as evidenced by the time spent in the target quadrant (Fig. 6h) & the number of platform crossings (Fig. 6i) in the PTZ cohort when compared to the control cohort. Significantly, UTI improved these indicators. In conclusion, the study reveals that in the PTZ-induced epilepsy model, heightened neuroinflammation, as evidenced by elevated levels of TNF-α, IL-1β, and IL-18, contributes to cognitive dysfunction. However, UTI treatment effectively suppresses inflammation, reduces cytokine production, and enhances learning and memory performance, thereby underscoring its potential as a therapeutic strategy to ameliorate cognitive impairments associated with epilepsy.

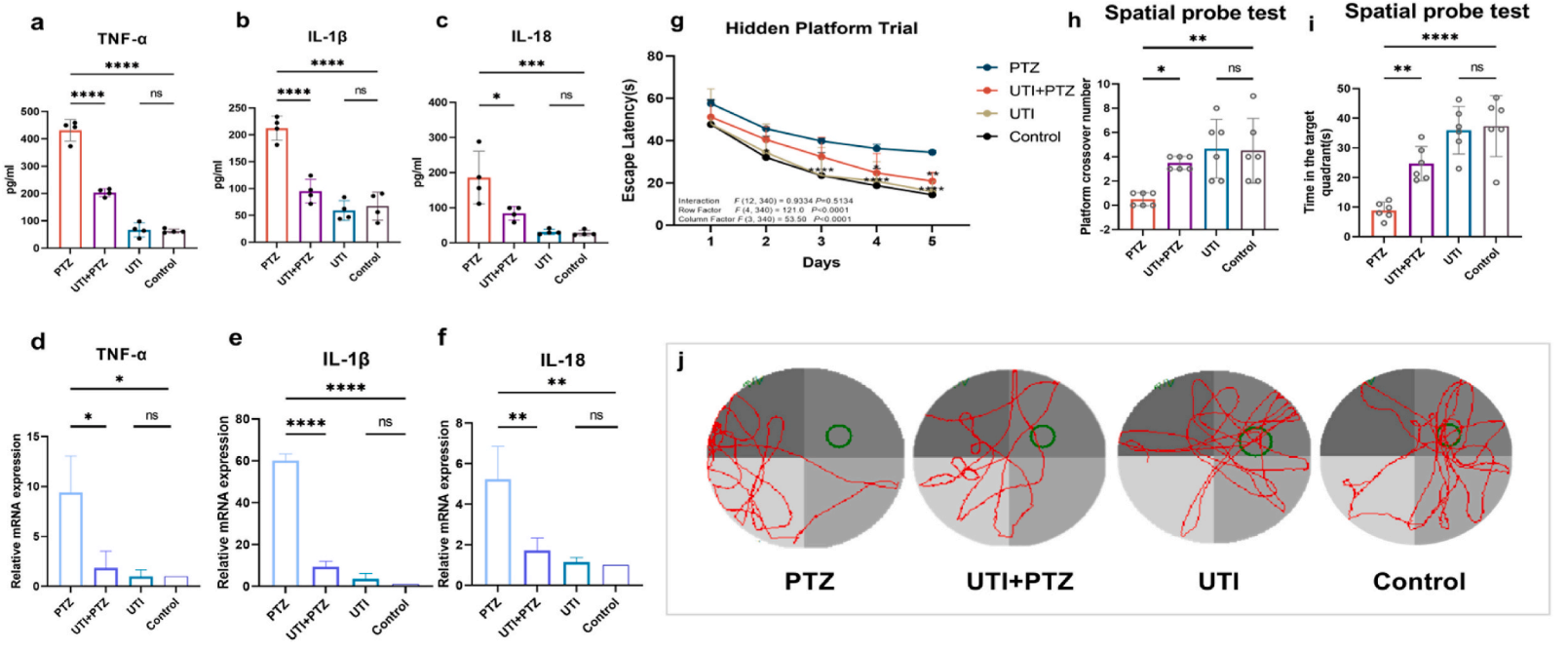

Fig. 6. Ulinastatin modulates inflammatory factor levels and cognitive function in the PTZ model.

a-c: TNF-α (a), IL-1β (b), & IL-18 (c) protein levels in peripheral serum were measured using ELISA. ns, P>0.05, *P<0.05, ***P<0.001, and ****P<0.0001. d-f: qPCR examination of the inflammatory cytokine mRNA expression in the hippocampal regions for TNF-α (d), IL-1β (e), & IL-18 (f). ns, P>0.05; * P<0.05; ** P<0.01; ****P<0.0001. Morris Water Maze: g: Evaluate the location navigation task's escape latencies. *P<0.05; **P<0.01; ****P<0.0001. Analysis of the number of platform crossings (h) and time spent in the target quadrant (i) in the spatial probe task. ns, P>0.05, *P<0.05, **P<0.01, and ****P<0.0001. j: Representative route tracing.

3.4. Ulinastatin Alleviates Pathological Changes in the PTZ Model

The PTZ group had a significantly higher proportion of Iba-1 positive microglia in the CA3 region of the hippocampus than the control as well as UTI groups ($P = 0.0094$), indicating significant microglial activation. This proportion decreased following UTI treatment ($P = 0.0476$, Fig. 7a). This information was revealed by immunohistochemical staining. In the same way, the PTZ group exhibited a noteworthy rise ($P < 0.001$) in GFAP-labeled astrocytes in the CA3 region of the hippocampus, while the UTI-treated group displayed a significant reduction ($P < 0.001$, Fig. 7b) in the positive cell area, suggesting that reactive astrocytosis occurred in the PTZ group while UTI may have inhibited neuroglial proliferation. The DG area of the hippocampal region, which is frequently the site of neural network reorganisation and mossy fibre sprouting, was the subject of quantitative and statistical analysis of NeuN-labeled neurons. The findings revealed that there were no statistically significant variations between the groups ($P > 0.05$, Fig. 7c), suggesting the absence of substantial neurogenesis or neuronal loss in this area. In summary, the PTZ-induced epilepsy group demonstrated heightened microglial activation and astrocytosis in the CA3 region of the hippocampus, which were attenuated by UTI

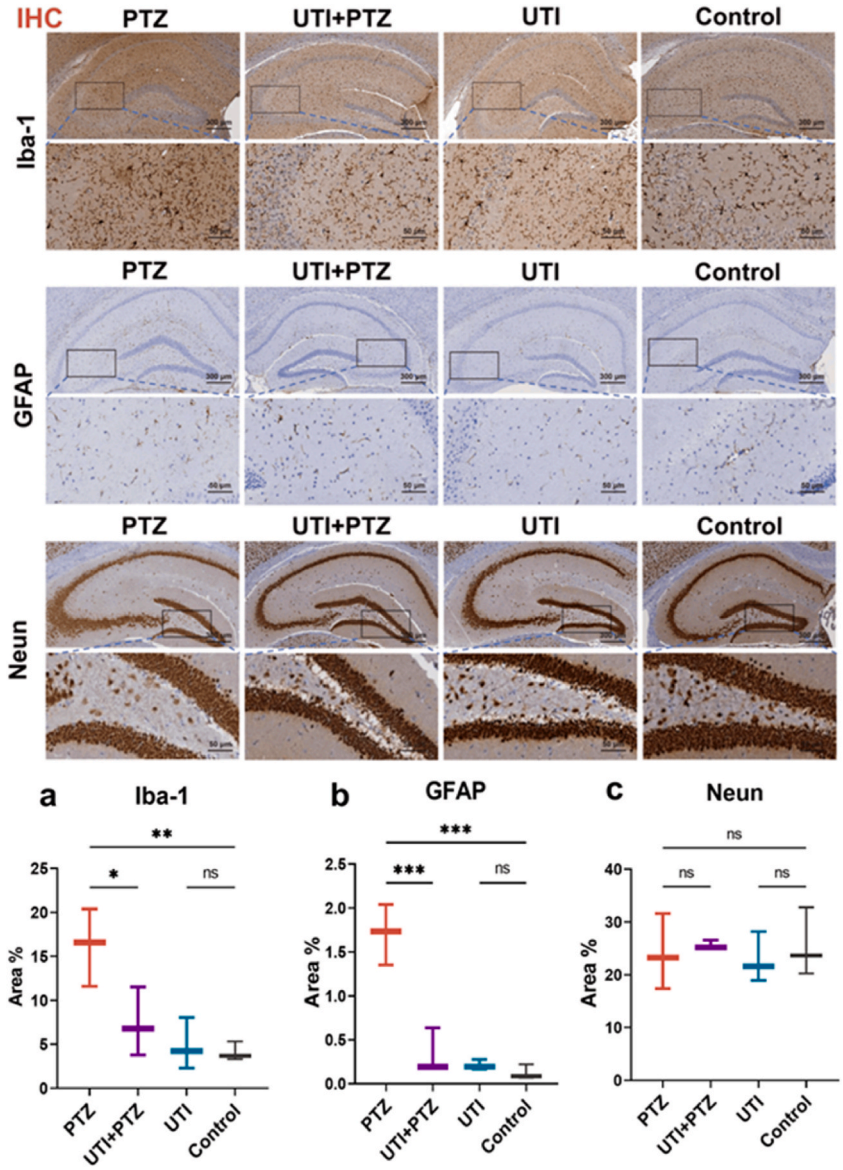

Fig. 7. Immunohistochemical Evaluation of neurocellular interactions Post-UTI treatment.
Quantitative analysis of neuronal biomarkers in hippocampal tissue using immunohistochemistry (IHC): aThe percentage of Iba-1-positive microglial cells in the CA3 region. b. region% representing the fraction of GFAP-positive astrocytes in the CA3 region. c. Dentate gyrus (DG) area percentage of NeuN-positive neurons. The data are displayed as mean ± standard deviation for all $n \geq 3$. **$P < 0.01$, ***$P < 0.001$, ****$P < 0.0001$, ns, $P > 0.05$. Scale bars: Hippocampus = 300 μm, other regions = 50 μm.

therapy, whereas the DG region showed no significant differences in neuronal density, implying preservation of neurogenesis or neuronal integrity.

3.5. Ulinastatin fine-tunes NLRP3-Linked glutamate and blood-brain barrier integrity in the PTZ model

A glutamate assay kit has been employed to quantify the quantity of glutamate released in the epilepsy model produced by pentylenetetrazol (PTZ), revealing significantly elevated levels of glutamate in the PTZ model ($P < 0.001$), which were reduced following UTI treatment ($P < 0.001$) (Fig. 8a). Evans Blue dye leakage was significantly higher in the hippocampal regions of the PTZ group than in the control group ($P < 0.001$) in blood-brain barrier tests, whereas the UTI-treated cohort had lower Evans Blue content ($P = 0.0003$) (Fig. 8b). Additionally, the blood-brain barrier's (BBB) integrity was assessed by using Western blot analysis to measure the tight junction protein claudin-5 expression (Fig. 8c). The expression of Claudin-5 was markedly reduced in the PTZ treatment ($P < 0.001$), indicating BBB disruption, while UTI treatment led to an upregulation of this protein ($P = 0.0028$), highlighting its therapeutic potential in restoring BBB integrity. Taken together, PTZ-induced epilepsy resulted in glutamate overload and BBB disruption, but UTI treatment reduced glutamate levels and preserved claudin-5, suggesting its restorative effects on the BBB.

3.6. Ulinastatin dually modulates NLRP3 activation and promotes neuroprotection in HT22 neurons

The CCK-8 assay for HT22 neurotoxicity showed that when HT22 was exposed to CM produced by BV2 stimulated with a gradient of LPS and ATP concentrations, The reduction in cell viability was dose-dependent. On the other hand, following UTI intervention, HT22 neuronal viability greatly enhanced, particularly at doses of 1, 3, & 5 mM (Fig. 9a). The dose-response curve indicated that ATP at 5 mM nearly inhibited 50 % of the cell activity (Fig. 9b). Therefore, in the following studies, 5 mM ATP was chosen as the most effective dose to generate CM in combination with 1 μg/ml LPS, and then this CM was introduced into HT22 cells to form the BV2-HT22 co-culture model.

Western blot assessment was used to examine the presence of NF-κB and NLRP3 inflammasome proteins in HT22. Based on the findings, it can be shown that NF-κB was activated ($P = 0.0015$) in the LPS-ATP group. This activation is supported by a rise in the proportion of phosphorylated p65 to p65, as shown in Fig. 9c. The ASC ($P = 0.0028$) & NLRP3 ($P = 0.0062$) proteins, which are components of the NLRP3 inflammasome, were expressed at higher levels, and the ratio of cleaved Caspase-1 to pro-Caspase-1, its precursor, rose dramatically ($P < 0.001$) (Fig. 9d–f). Nevertheless, following UTI intervention, these alterations were reversed (all for $P < 0.05$), suggesting that UTI blocked the activation of this pathway in HT22. This investigation demonstrated that neurons and BV2 microglial cells both activate the NLRP3 inflammasome. Furthermore, BV2's action on HT22 directly causes neurogenic inflammation in addition to stimulating inflammatory factors to raise neuronal excitability in epilepsy.

Additionally, in a co-culture system simulating epilepsy-related neuroinflammation, Annexin V-FITC/PI apoptosis assays yielded results like the CCK8 experiments. In the model group stimulated with LPS and ATP (LPS-ATP group), In HT22 neurons, the corresponding rates of early & late apoptosis were 74.20 %, 66.51 %, & 65.26 %. After treatment with ulinastatin in the UTI-LPS-ATP group, the total apoptosis rates were significantly reduced to 37.5 %, 36.67 %, and 39.46 %, further confirming the neuroprotective efficacy of

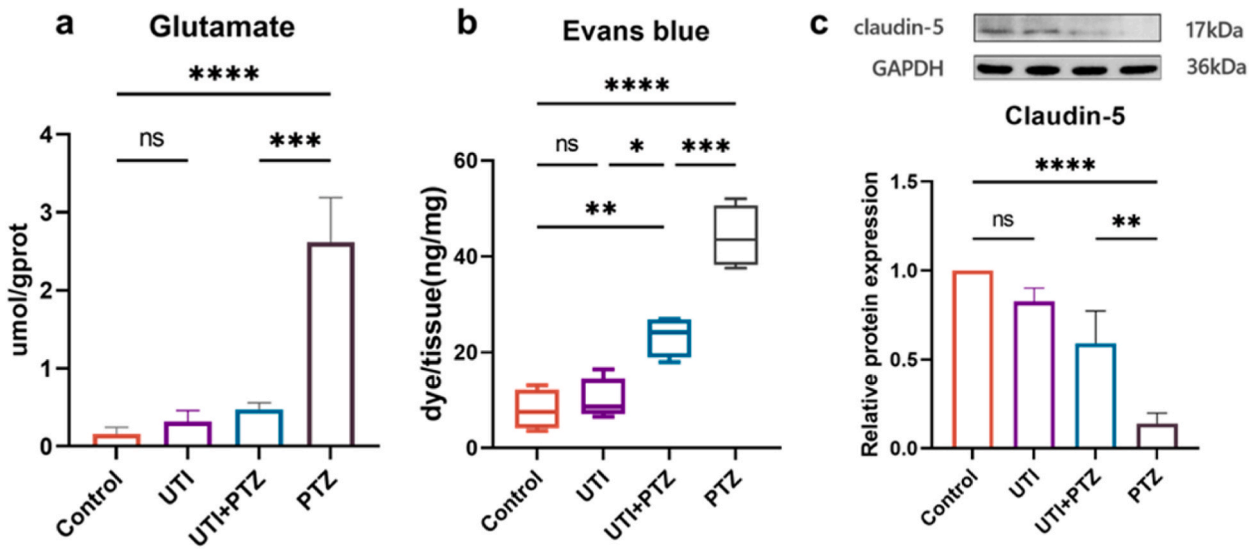

Fig. 8. UTI's impact on glutamate levels and blood-brain barrier function in epileptic mice.
a: Quantitative analysis of glutamate levels in hippocampal tissue. ***$P < 0.001$; ****$P < 0.0001$. b: Quantitative analysis of Evans Blue dye in brain tissue. ***$P < 0.001$; ****$P < 0.0001$. c: Western blot analysis of the relative protein expression of claudin-5. **$P < 0.01$; ****$P < 0.0001$. Data are presented as mean ± standard deviation ($n \geq 3$). The uncropped and full-size images for (Fig. 8c) this figure are provided in Supplementary Fig. S2.

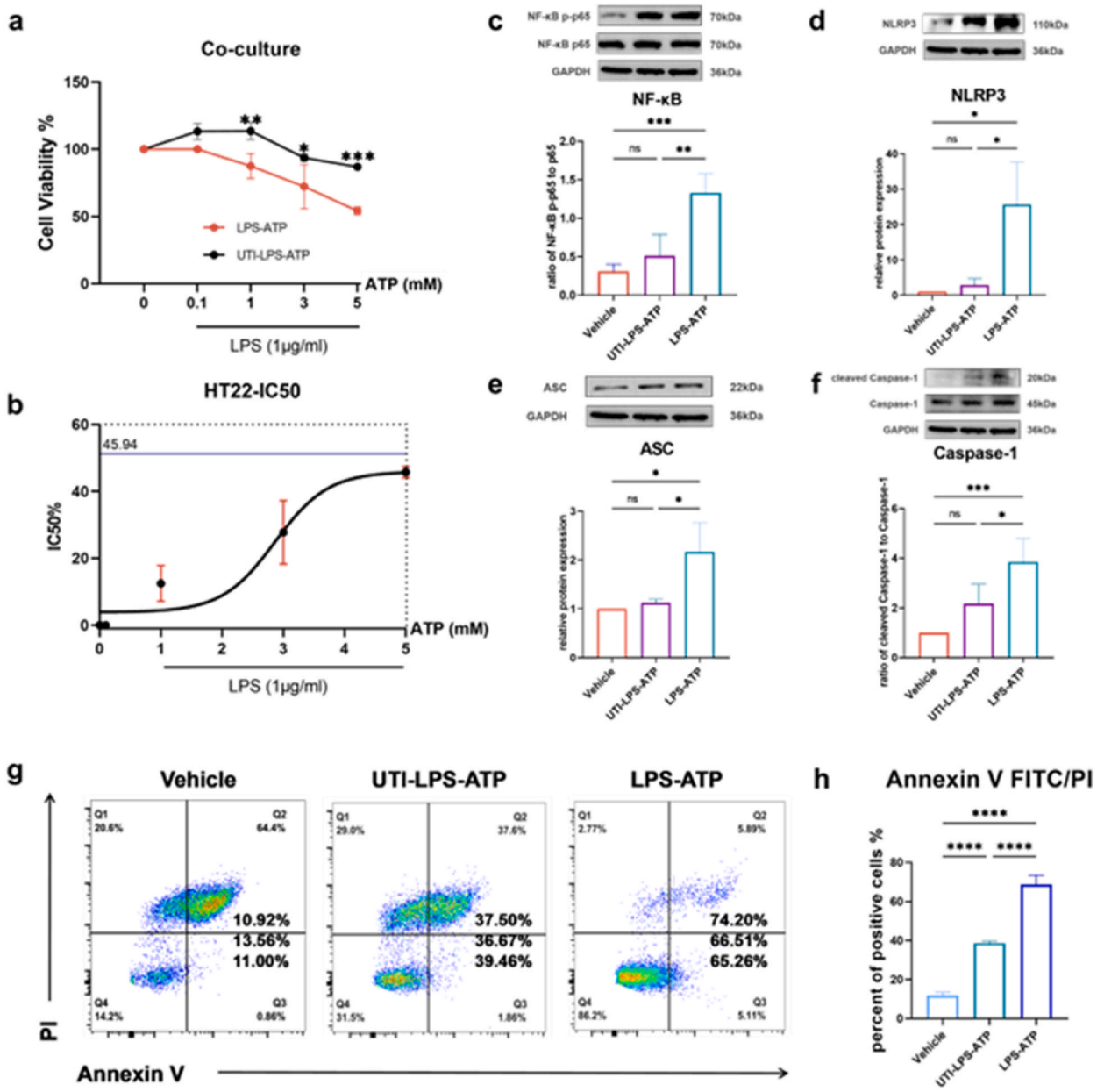

Fig. 9. The impact of UTI on the BV2-HT22 Co-culture model.
(a)CCK8 assay evaluating the impact of ulinastatin on cell viability in the LPS and ATP-induced BV2-HT22 co-culture model, $^{*}P < 0.05$; $^{**}P < 0.01$; $^{***}P < 0.001$. (b) CCK8 assay plotting the dose-response curve with IC50 for HT22 neurons. Western blot quantification in BV2-HT22 co-cultured cells. (c) Ratio of phosphorylated to non-phosphorylated NF-κB p65, $^{**}P < 0.01$; $^{***}P < 0.001$. (d) Relative protein expression of NLRP3, $^{*}P < 0.05$. (e) Relative protein expression of ASC, $^{*}P < 0.05$. (f) Ratio of cleaved Caspase-1 to total Caspase-1, $^{*}P < 0.05$, $^{***}P < 0.001$. (g) FlowJo flow cytometry profile stained with Annexin V FITC/PI. (h) Quantitative analysis of the total apoptosis rate (early plus late apoptosis) in HT22 neurons in the co-culture model, $^{****}P < 0.0001$. Data are presented as mean ± standard deviation ($n \geq 3$).
The uncropped and full-size images for (Fig. 9c–d) this figure are provided in Supplementary Fig. S3.

ulinastatin in rescuing neurons (Fig. 9g–h). Together, neuroinflammation triggered by microglial activation in epilepsy was found to involve the NLRP3 inflammasome and NF-κB, leading to neuronal damage. UTI treatment showed potential to mitigate these effects and protect neurons.

4. Discussion

Epilepsy, a multifaceted neurological disorder affecting the central nervous system (CNS), poses significant challenges due to its

association with cognitive decline and substantial disability-adjusted life years (DALYs) [32]. The intricate interplay between inflammation and epilepsy has garnered increasing attention, particularly the pivotal role played by the NLRP3 inflammasome in orchestrating pro-inflammatory immune responses [33,35]. Empirical evidence from clinical and preclinical studies underscores the therapeutic potential of targeting inflammasome signaling cascades in epilepsy management [33]. Empirical evidence from clinical and preclinical studies underscores the therapeutic potential of targeting inflammasome signaling cascades in epilepsy management [34]. Our study pioneers an extensive investigation into UTI's impact on epilepsy, both in vitro and in vivo, revealing its unique capacity to inhibit the NLRP3 inflammasome pathway, thereby attenuating epileptogenesis, mitigating neuroinflammation, enhancing cognitive performance, modulating neuroglial interactions, facilitating blood-brain barrier restoration, and regulating glutamate levels, collectively demonstrating its neuroprotective attributes. The rationale behind the utilization of UTI stems from its multifaceted action on the NF-κB/NLRP3 axis and its cognitive-enhancing properties, directly addressing the complex etiology of epilepsy.It is well utilizing that proper brain development & preservation of brain homeostasis depend heavily on the immune microenvironment and related inflammatory mediators. In epilepsy patients, neuroinflammation is often aseptic, triggered by neurogenic inflammation leading to neuronal hyperactivity and recurrent seizuresInflammatory cns reactions in response to neuronal activity. In the context of epilepsy, neuroinflammationtypically arises from asterile process, ignitedby neuron-derived inflammation, which fostersexcessive neuronal excitabilityand recurrent seizures [35]. The main contributors to neuroinflammation are glial cells, which participate in a complex pro-inflammatory and anti-inflammatory signaling network within the immune microenvironment by activating innate immune mechanisms and releasing inflammatory mediators [36]. These dynamic processes play a pivotal role in shaping neuronal function across the lifespan and are indispensable for the formation and refinement of neural networks during brain development [37]. This understanding underscores the importance of targeting neuroinflammatory pathways, such as the NLRP3 inflammasome, for therapeutic intervention in epilepsy, as it could potentially alleviate inflammation, restore brain homeostasis, and mitigate seizure recurrence. Ulinastatin, by inhibiting the NLRP3 inflammasome, emerges as a promising strategy in this regard, targeting the multi-faceted aspects of epilepsy pathophysiology.

Steroids, which have broad-spectrum immunomodulatory and anti-inflammatory qualities, have been used in clinical studies for a long time to treat drug-resistant epilepsy, including autoimmune limbic encephalitis [38], severe paediatric seizures, as well as super-refractory status epilepticus [39]. Their anti-inflammatory properties that influence neuronal excitability are thought to mediate their effectiveness. Using anakinra, a human recombinant IL-1R1 antagonist, or caspase-1 inhibitors, an IL-1β biosynthesis enzyme, to block the IL-1β/IL-1R1 axis in rat models of status epilepticus or post-traumatic epilepsy [40], or targeting the ATP-P2X7 receptor axis [41], or other anti-inflammatory drugs [42,43] have all resulted in seizure control. In our study, we found that UTI improved seizure scores and latency in PTZ-induced epileptic mice by inhibiting NLRP3 inflammasome activation in brain cells, demonstrating its anti-epileptogenic effect. Concurrently, UTI reduced hippocampal and systemic inflammatory responses, consistent with previous findings [44,45]. Compelling evidence indicates that ictogenic cytokines, such as IL-1β, can reduce GABAAR-mediated current amplitudes in the hippocampus of TLE patients & rodents [46,47]. In our investigation, the hippocampal IL-1β levels were considerably lowered by UTI.

The benefits of anti-inflammatory therapy in rodent and clinical studies include reducing neurocomorbidities and neuropathology, primarily depending on timely intervention during disease progression [46]. Cognitive impairment in a variety of neurological illnesses, including epilepsy, is attributed to the molecular and cellular activation of microglia and astrocytes by the NLRP3 inflammasome [48,49]. Brain cells that express similar receptors & signalling pathways, such as neurons, glial cells, & cerebrovascular endothelial systems, can trigger autocrine & paracrine responses after the release of pro-inflammatory mediators during neuroinflammation. Under physiological settings, different cytokines and chemokines affect synaptic transmission. For example, TNF and IL-1β play important roles in synaptic plasticity, which is the basis for memory and learning [50].

In our study, UTI improved cognitive function in epileptic animals through its anti-inflammatory effects. IHC labelling was used in the neuropathological study to verify that UTI lowered microglia-astrocyte interaction in the hippocampal regions of epileptic animals, hence reducing the high glutamate levels that were previously present. However, previous studies have indicated that neurogenesis may occur in the hippocampal region of PTZ-induced epilepsy models during late stages of multiple low-dose PTZ administration, primarily characterized by increased NeuN expression in CA1, CA3, & DG regions [51,52], promoted by M2-type microglia [53]. In our study, this phenomenon was not observed, potentially due to differences in PTZ administration regimens or microglial M1/M2 polarization. Nevertheless, this study did not involve M1/M2 microglial phenotyping.

In epilepsy, glial cell neuroinflammation is linked to changes in the blood-brain barrier's integrity. Important elements of the blood-brain barrier are tight junctions, which are formed by endothelial cells expressing Claudin-5, which is encoded by the CLDN5 gene [54]. Downregulation of claudin-5 expression leads to serum albumin extravasation [55,56], further activating glial cell signaling, affecting homeostatic genes, lowering the seizure threshold, and contributing to drug resistance mechanisms and neurodegenerative changes. In rodent models, rapamycin can upregulate tight junction proteins, restore blood-brain barrier integrity, and control seizures [57]. Although medication resistance was not examined, our work discovered that UTI increased the expression of the claudin-5 protein in the hippocampal regions of epileptic mice, supporting its function in blood-brain barrier repair.

Prior research has shown that the NLRP3 inflammasome is predominantly found in microglia; however, brain tissue from TLE patients and mice models of pilocarpine-induced epilepsy have demonstrated its activation in both microglia and neurons [57]. In vitro, our BV2-HT22 co-culture studies yielded consistent results with in vivo experiments, showing that microglial stimulation induced neurogenic inflammation and activated the NF-κB/NLRP3 pathway in neurons, avoiding direct intervention with NF-κB and NLRP3 agonists in HT22 neurons. The CCK8 test gradients of ATP concentration verified a favourable correlation between neuronal survival and the degree of NLRP3 pathway activation in microglia. Annexin V assay further revealed that UTI could inhibit inflammatory signaling pathways in neurons, preventing neuronal death.

The study limitations include the incomplete understanding of the exact molecular mechanism behind UTI's action on the NLRP3 inflammasome, potential confounding variables in the in vivo model, and the necessity for validation in human studies to ensure translatability of our findings. Further research is needed to address these limitations and fully establish UTI's therapeutic potential in epilepsy.

In conclusion, our study provides strong evidence for the therapeutic potential of UTI in dampening neuroinflammation and ameliorating cognitive dysfunction associated with epilepsy. The observed anti-inflammatory and neuroprotective effects support further exploration of UTI as a novel treatment option in epilepsy, complementing current approaches and contributing to the development of more effective therapies.

5. Conclusion

In conclusion, our study demonstrates that in a mouse model of epilepsy, Ulinastatin (UTI) can counteract seizures and neuroinflammation by inhibiting the NLRP3 signaling pathway, improving cognitive function and blood-brain barrier integrity, and reducing glutamate release, proving the necessity of these effects in epilepsy. In the BV2-HT22 neuron co-culture system, UTI alleviated microglia-neuron interactions and increased neuronal survival by inhibiting the NLRP3 signaling pathway. Although the detailed mechanisms remain to be elucidated, preliminary findings suggest that UTI's neuroprotective effects are mediated through the regulation of the NLRP3 inflammasome. Due to its low toxicity, side effects, and multifaceted pharmacological effects, as well as its widespread clinical application, UTI provides significant medical value for epilepsy treatment.

Funding

The National Natural Science Foundation of China (Nos. 30872791) provided funding for this work & the Harbin Medical University Pediatric Academic Staff Funding Project (Nos. 31021220021).

Data and materials availability

The data used to support this study are available from the corresponding author upon request.

Ethical statement

This research adhered to the ethical guidelines of Harbin Medical University's First Affiliated Hospital. Animal procedures aimed to reduce distress & obtained the Institutional Animal Care and Use Committee's permission. (Approval No. LACUC:2021127).

Consent for publication

Not relevant since there was no personal or human participant data used in this study.

CRediT authorship contribution statement

Huan Wang: Validation, Methodology, Investigation, Formal analysis, Data curation. **Yuzhu Ma:** Methodology, Investigation, Data curation, Conceptualization. **Dongmei Jin:** Writing – review & editing, Writing – original draft, Methodology, Investigation. **Xinlei Yang:** Methodology, Investigation, Formal analysis, Data curation. **Xiangping Xu:** Supervision, Methodology, Investigation, Formal analysis.

Declaration of competing interest

The authors declare that they have no known competing financial interests or personal relationships that could have appeared to influence the work reported in this paper.

Appendix A. Supplementary data

Supplementary data to this article can be found online at https://doi.org/10.1016/j.heliyon.2024.e38050.

References

[1] R.D. Thijs, et al., Epilepsy in adults, Lancet 393 (10172) (2019) 689–701.
[2] Y. Liew, et al., Neuroinflammation: a common pathway in alzheimer's disease and epilepsy, J Alzheimers Dis 94 (s1) (2023) S253–s265.
[3] S. Tripathi, et al., The immune system and metabolic products in epilepsy and glioma-associated epilepsy: emerging therapeutic directions, JCI Insight 9 (1) (2024).

[4] G. Yamanaka, et al., Links between immune cells from the periphery and the brain in the pathogenesis of epilepsy: a narrative review, Int. J. Mol. Sci. 22 (9) (2021).
[5] M.K. Jha, et al., Microglia-astrocyte crosstalk: an intimate molecular conversation, Neuroscientist 25 (3) (2019) 227–240.
[6] C. Twible, et al., Astrocyte role in temporal lobe epilepsy and development of mossy fiber sprouting, Front. Cell. Neurosci. 15 (2021) 725693.
[7] E.A. van Vliet, N. Marchi, Neurovascular unit dysfunction as a mechanism of seizures and epilepsy during aging, Epilepsia 63 (6) (2022) 1297–1313.
[8] M. Zheng, T.D. Kanneganti, The regulation of the ZBP1-NLRP3 inflammasome and its implications in pyroptosis, apoptosis, and necroptosis (PANoptosis), Immunol. Rev. 297 (1) (2020) 26–38.
[9] H. Sharif, et al., Structural mechanism for NEK7-licensed activation of NLRP3 inflammasome, Nature 570 (7761) (2019) 338–343.
[10] K.V. Swanson, et al., The NLRP3 inflammasome: molecular activation and regulation to therapeutics, Nat. Rev. Immunol. 19 (8) (2019) 477–489.
[11] E. Cristina de Brito Toscano, et al., NLRP3 and NLRP1 inflammasomes are up-regulated in patients with mesial temporal lobe epilepsy and may contribute to overexpression of caspase-1 and IL-β in sclerotic hippocampi, Brain Res. 1752 (2021) 147230.
[12] C. Wu, et al., The role of NLRP3 and IL-1β in refractory epilepsy brain injury, Front. Neurol. 10 (2019) 1418.
[13] A. Samadianzakaria, et al., The effect of valproic acid and furosemide on the regulation of the inflammasome complex (NLRP1 and NLRP3 mRNA) in the brain of epileptic animal model, Brain Res. Bull. 191 (2022) 20–29.
[14] L. Palumbo, et al., The NLRP3 inflammasome in neurodegenerative disorders: insights from epileptic models, Biomedicines 11 (10) (2023).
[15] X. Wang, et al., DHA and EPA prevent seizure and depression-like behavior by inhibiting ferroptosis and neuroinflammation via different mode-of-actions in a pentylenetetrazole-induced kindling model in mice, Mol. Nutr. Food Res. 66 (22) (2022) e2200275.
[16] X.F. Meng, et al., Inhibition of the NLRP3 inflammasome provides neuroprotection in rats following amygdala kindling-induced status epilepticus, J. Neuroinflammation 11 (2014) 212.
[17] A.D. DeSena, et al., Systemic autoinflammation with intractable epilepsy managed with interleukin-1 blockade, J. Neuroinflammation 15 (1) (2018) 38.
[18] J. Li, et al., Efficacy analysis of oral dexamethasone in the treatment of infantile spasms and infantile spasms related Lennox-Gastaut syndrome, BMC Pediatr. 23 (1) (2023) 255.
[19] R. Matsuura, et al., Long-term analysis of adrenocorticotropic hormone monotherapy for infantile epileptic spasms syndrome with periventricular leukomalacia, Seizure 109 (2023) 40–44.
[20] K. Wang, et al., Amomum tsaoko fruit extract exerts anticonvulsant effects through suppression of oxidative stress and neuroinflammation in a pentylenetetrazol kindling model of epilepsy in mice, Saudi J. Biol. Sci. 28 (8) (2021) 4247–4254.
[21] M.J. Pugia, et al., Bikunin (urinary trypsin inhibitor): structure, biological relevance, and measurement, Adv. Clin. Chem. 44 (2007) 223–245.
[22] R.E. Abo El Gheit, et al., Role of serine protease inhibitor, ulinastatin, in rat model of hepatic encephalopathy: aquaporin 4 molecular targeting and therapeutic implication, J. Physiol. Biochem. 76 (4) (2020) 573–586.
[23] M. Feng, et al., Ulinastatin attenuates experimental autoimmune encephalomyelitis by enhancing anti-inflammatory responses, Neurochem. Int. 64 (2014) 64–72.
[24] R. Guo, et al., Ulinastatin attenuates spinal cord injury by targeting AMPK/NLRP3 signaling pathway, J. Chem. Neuroanat. 125 (2022) 102145.
[25] Y.S. Kim, et al., Protective effect of ulinastatin on cognitive function after hypoxia, NeuroMolecular Med. 25 (1) (2023) 136–143.
[26] X. Li, et al., Ulinastatin downregulates TLR4 and NF-kB expression and protects mouse brains against ischemia/reperfusion injury, Neurol. Res. 39 (4) (2017) 367–373.
[27] J. Qiu, et al., Ulinastatin protects against sepsis-induced myocardial injury by inhibiting NLRP3 inflammasome activation, Mol. Med. Rep. 24 (4) (2021).
[28] W. Tan, et al., TNF-α is a potential therapeutic target to overcome sorafenib resistance in hepatocellular carcinoma, EBioMedicine 40 (2019) 446–456.
[29] H. Zhang, et al., NLRP3 inflammasome involves in the pathophysiology of sepsis-induced myocardial dysfunction by multiple mechanisms, Biomed. Pharmacother. 167 (2023) 115497.
[30] T. Shimada, K. Yamagata, Pentylenetetrazole-induced kindling mouse model, J. Vis. Exp. 136 (2018).
[31] Y. Hong, et al., Ulinastatin alleviates repetitive ketamine exposure-evoked cognitive impairment in adolescent mice, Neural Plast. 2022 (2022) 6168284.
[32] J. Chen, et al., Mechanism of NLRP3 inflammasome in epilepsy and related therapeutic agents, Neuroscience 546 (2024) 157–177.
[33] M.S. Pohlentz, et al., Characterisation of NLRP3 pathway-related neuroinflammation in temporal lobe epilepsy, PLoS One 17 (8) (2022) e0271995.
[34] A. Vezzani, et al., Neuroinflammatory pathways as treatment targets and biomarkers in epilepsy, Nat. Rev. Neurol. 15 (8) (2019) 459–472.
[35] A. Vezzani, et al., IL-1 receptor/Toll-like receptor signaling in infection, inflammation, stress and neurodegeneration couples hyperexcitability and seizures, Brain Behav. Immun. 25 (7) (2011) 1281–1289.
[36] P.A. Garay, A.K. McAllister, Novel roles for immune molecules in neural development: implications for neurodevelopmental disorders, Front. Synaptic Neurosci. 2 (2010) 136.
[37] A. Vezzani, et al., Astrocytes in the initiation and progression of epilepsy, Nat. Rev. Neurol. 18 (12) (2022) 707–722.
[38] A. Vincent, et al., The growing recognition of immunotherapy-responsive seizure disorders with autoantibodies to specific neuronal proteins, Curr. Opin. Neurol. 23 (2) (2010) 144–150.
[39] T.H. Tan, et al., Inflammation, ictogenesis, and epileptogenesis: an exploration through human disease, Epilepsia 62 (2) (2021) 303–324.
[40] M. Maroso, et al., Toll-like receptor 4 and high-mobility group box-1 are involved in ictogenesis and can be targeted to reduce seizures, Nat. Med. 16 (4) (2010) 413–419.
[41] A. Jimenez-Pacheco, et al., Transient P2X7 receptor antagonism produces lasting reductions in spontaneous seizures and gliosis in experimental temporal lobe epilepsy, J. Neurosci. 36 (22) (2016) 5920–5932.
[42] Y.S. Kwon, et al., Neuroprotective and antiepileptogenic effects of combination of anti-inflammatory drugs in the immature brain, J. Neuroinflammation 10 (2013) 30.
[43] X. Ping, et al., Blocking receptor for advanced glycation end products (RAGE) or toll-like receptor 4 (TLR4) prevents posttraumatic epileptogenesis in mice, Epilepsia 62 (12) (2021) 3105–3116.
[44] R. Liu, et al., Ibuprofen exerts antiepileptic and neuroprotective effects in the rat model of pentylenetetrazol-induced epilepsy via the COX-2/NLRP3/IL-18 pathway, Neurochem. Res. 45 (10) (2020) 2516–2526.
[45] C. Ulusoy, et al., Peripheral blood expression levels of inflammasome complex components in two different focal epilepsy syndromes, J. Neuroimmunol. 347 (2020) 577343.
[46] C. Roseti, et al., GABAA currents are decreased by IL-1β in epileptogenic tissue of patients with temporal lobe epilepsy: implications for ictogenesis, Neurobiol. Dis. 82 (2015) 311–320.
[47] S. Wang, et al., Interleukin-1beta inhibits gamma-aminobutyric acid type A (GABA(A)) receptor current in cultured hippocampal neurons, J. Pharmacol. Exp. Therapeut. 292 (2) (2000) 497–504.
[48] A. Altmann, et al., A systems-level analysis highlights microglial activation as a modifying factor in common epilepsies, Neuropathol. Appl. Neurobiol. 48 (1) (2022) e12758.
[49] M. Santello, et al., Astrocyte function from information processing to cognition and cognitive impairment, Nat. Neurosci. 22 (2) (2019) 154–166.
[50] A. Vezzani, B. Viviani, Neuromodulatory properties of inflammatory cytokines and their impact on neuronal excitability, Neuropharmacology 96 (Pt A) (2015) 70–82.
[51] H. Sahin, et al., Protective effects of intranasally administrated oxytocin-loaded nanoparticles on pentylenetetrazole-kindling epilepsy in terms of seizure severity, memory, neurogenesis, and neuronal damage, ACS Chem. Neurosci. 13 (13) (2022) 1923–1937.
[52] M. Shahpari, et al., Improved stage categorization of PTZ-induced kindling and late enhanced neurogenesis in PTZ kindled mice, Galen Med J 8 (2019) e1511.
[53] A.M. Nikolakopoulou, et al., Activated microglia enhance neurogenesis via trypsinogen secretion, Proc Natl Acad Sci U S A 110 (21) (2013) 8714–8719.
[54] H. Chiba, et al., The region-selective regulation of endothelial claudin-5 expression and signaling in brain health and disorders, J. Cell. Physiol. 236 (10) (2021) 7134–7143.

[55] J.A. Gorter, et al., The roof is leaking and a storm is raging: repairing the blood-brain barrier in the fight against epilepsy, Epilepsy Curr. 19 (3) (2019) 177–181.
[56] W. Löscher, A. Friedman, Structural, molecular, and functional alterations of the blood-brain barrier during epileptogenesis and epilepsy: a cause, consequence, or both? Int. J. Mol. Sci. 21 (2) (2020).
[57] P. Xie, et al., Rapamycin plays an anti-epileptic role by restoring blood-brain barrier dysfunction, balancing T cell subsets and inhibiting neuronal apoptosis, Discov. Med. 35 (179) (2023) 1043–1051.